Registration of Magnetic Resonance Images of the Prostate Obtained with an Endorectal Coil to Histological Sections

Y. Mazaheri[1], O. Akin[2], A. Shukla-Dave[1], D. Chamudot[1], L. Wang[2], J. Grater[1], S. W. Fine[3], V. Reuter[3], J. A. Koutcher[1], and H. Hricak[2]

[1]Medical Physics, Memorial Sloan Kettering Cancer Center, New York, NY, United States, [2]Radiology, Memorial Sloan Kettering Cancer Center, New York, NY, United States, [3]Pathology, Memorial Sloan Kettering Cancer Center, New York, NY, United States

Introduction

Validation of findings from *in vivo* imaging (e.g. MRI) of the prostate requires precise correlation of histopathological information on a voxel-by-voxel basis, with sub-millimeter accuracy in the absence of identifiable anatomic landmarks. A method is developed to register histopathology sections and *in vivo* MR images of the prostate obtained with a combination of a phased-array and an endodrectal coil. Previous relevant work includes co-registration and warping of MR images to histolopathologic sections using nonlinear thin-plate splines in small animal studies (1) and co-registration of histolopathological and MR images of the prostate using both boundary and internal landmarks with thin-plate splines (2). Here we present a 2D semiautomatic nonrigid registration using free-form deformation (FFD) based on B-splines (3) to co-register MR images to histopathological sections. Landmarks are used to match the corresponding MR images and histopathological slides.

Methods

Imaging: The MRI exam was performed on 40 patients with a 1.5-T whole-body MRI unit (GE Medical Systems, Milwaukee, WI). A body coil was used for excitation, and a pelvic four-channel phased-array coil combined with a commercially available balloon-covered expandable endorectal coil (ERC) (Medrad, Pittsburgh, PA) was used for signal reception. TheERC coil was inflated with 60-100 ml of air. Appropriate positioning of the coil is decided based on good craniocaudal coverage of the prostate and seminal vesicles and whether the coil is positioned such that bright spots on the localization images are oriented parallel to the table (i.e. the coil has not been rotated). As per the standard clinical prostate MRI examination at our institution, the images obtained included transverse T1-w images and transverse, coronal, and sagittal T2-w fast spin-echo images of the prostate.

Histopathological Analysis: The specimens were step-sectioned into 3–5-mm slices after prostate resection as previously described (4). The cancer foci were outlined in color inks to denote Gleason score (green = Gleason grade $\leq$ 3; black = Gleason grade 4 or 5), presence of extraprostatic extension (blue), and margin positivity (red) on whole-mount step-section pathologic slices of the prostate so as to be grossly visible before being digitally scanned.

Image Co- registration: Axial MR images of human prostate obtained *in vivo* were co-registered to the corresponding sections of hematoxylin-and-eosin-stained (H&E) histopathological slides in 2 steps:

Step 1: Whole-mount step-section pathologic slices were matched with the corresponding T2-w images by a radiologist on the basis of anatomical landmarks, including the presence of urinary bladder and seminal vesicle tissue in superior slices, the slice with the largest diameter, progressive changes in the diameter of the slices, the thickness of the peripheral zone, the position of the pseudocapsule, and the presence, size, and shape of the transition zone.

Step 2: On both the pathology slide and the corresponding MR image closed contours were drawn manually. Deformable registration was performed on the contour images using the FFD method developed by Rueckert (3) and implemented in Matlab. In brief, the algorithm creates an underlying mesh of control points; the mesh is deformed based on B-splines. The extent of nonrigid deformation depends on the resolution of the control points. A similarity criterion is used to measure the degree of alignment. Here we have used normalized mutual information for similarity measurements. To evaluate the performance of the technique, prostate areas measured before and after warping on MR were compared to pathology and the percentage differences were calculated. The B-splines' FFD was defined by a 10×10 grid of control points. The algorithm was implemented as an iterative multi-resolution analysis (coarse-to-fine). At each iteration, the control point resolution and image resolution are increased. The number of iterations was 15. The accuracy of the image registration was measured using the Dice Similarity Coefficient (D) defined as $D = \frac{2a}{2a+b+c}$, where a is the number of voxels shared by both areas, b is the number of voxels unique to the 1st area (pathology), and c is the number of voxels unique to the 2nd area (5).

Results

Fig. 1 is a demonstration of the co-registration between an MR image (2D T2-w image) and a whole-mount step-section histopathologic section of a prostate gland. Prostate area measured on a single histopathologic section (Fig. 1A) was 5.09 cm^2; on the corresponding T2-w image, the prostate area was 5.46 cm^2 (Fig. 1B) before warping and 5.15 cm^2 after warping (Fig. 1E). D was 0.81 before warping and D_{warp} was 0.98 (after warping).

Discussion

We present a method for retrospective co-registration of MRI to histopathology that does not require the use of external markers during imaging. The results suggest good alignment of MR images to histological sections (Fig. 1E). Heijmink et al reported a significant decrease in the shape and total volume of the prostate caused by the introduction of the ERC (6). Eichelberger et al. (7) measured tissue shrinkage during tissue processing. In our study, by using a FFD method for co-registration of ERC MR images to histolopathologic sections, we account for both tissue shrinkage (pathology) and prostate deformation due to placement of the ERC (MRI). The methodology could be useful in studies that require precise maping on a voxel-by-voxel basis of *in vivo* findings (such as new imaging markers and/or multimodal imaging) onto histopathologic sections.

References: [1] Jacobs MA, *et al*. Med Phys 1999; 26:1568-1578. [2] Zhan Y, *et al*. Acad Radiol 2007; 14:1367-1381. [3] Rueckert D, *et al*. IEEE Trans Med Imaging 1999; 18:712-721. [4] Yossepowitch O, *et al.* J Urol 2002; 168:2011-2015. [5] Alterovitz R, *et al.* Med. Phys. 2006; 33:446-454. [6] Heijmink SW, *et al*. ISMRM; 2008:2771. [7] Eichelberger LE, *et al*. Am J Clin Pathol. 2003;120(3):386-91.

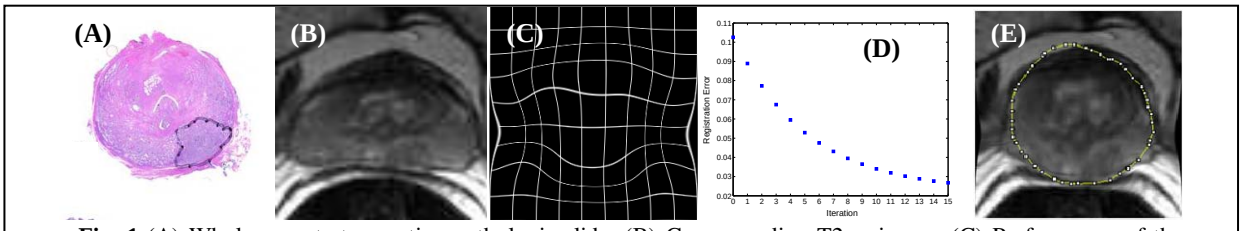

Fig. 1:(A) Whole-mount step-section pathologic slide. (B) Corresponding T2-w image. (C) Performance of the deformable warping visualized by deforming a regular grid (D) Plot of the error registration of the grid-points as a function of iteration. (E) Resulting warped T2-w image. The boundries of the pathology slide are overlaid.